Josephson radiation and shot noise of a semiconductor nanowire junction

David J. van Woerkom,[1,2] Alex Proutski,[1,2] Ruben J. J. van Gulik,[1,2] Tamás Kriváchy,[1,2] Diana Car,[3] Sébastian R. Plissard,[2,3] Erik P. A. M. Bakkers,[1,2,3] Leo P. Kouwenhoven,[1,2] and Attila Geresdi[1,2,*]

[1]*QuTech, Delft University of Technology, 2600 GA Delft, The Netherlands*

[2]*Kavli Institute of Nanoscience, Delft University of Technology, 2600 GA Delft, The Netherlands*

[3]*Department of Applied Physics, Eindhoven University of Technology, 5600 MB Eindhoven, The Netherlands*

(Received 10 February 2017; revised manuscript received 24 July 2017; published 11 September 2017)

We measured the Josephson radiation emitted by an InSb semiconductor nanowire junction utilizing photon-assisted quasiparticle tunneling in an ac-coupled superconducting tunnel junction. We quantify the action of the local microwave environment by evaluating the frequency dependence of the inelastic Cooper-pair tunneling of the nanowire junction and find the zero-frequency impedance $Z(0) = 492\ \Omega$ with a cutoff frequency of $f_0 = 33.1$ GHz. We extract a circuit coupling efficiency of $\eta \approx 0.1$ and a detector quantum efficiency approaching unity in the high-frequency limit. In addition to the Josephson radiation, we identify a shot noise contribution with a Fano factor $F \approx 1$, consistently with the presence of single electron states in the nanowire channel.

DOI: 10.1103/PhysRevB.96.094508

The tunneling of Cooper pairs through a junction between two superconducting condensates gives rise to a dissipationless current [1] with a maximum amplitude of the critical current, I_c [2]. Upon applying a finite voltage bias V, the junction becomes an oscillating current source

$$I_s(t) = I_c \sin(2\pi f t), \tag{1}$$

with a frequency set by $hf = 2eV$ where h is the Planck constant and e is the electron charge.

The Josephson radiation, defined by Eq. (1) has mostly been investigated for superconducting tunnel junctions [3–5], metallic Cooper-pair transistors [6], and in circuit QED geometries [7,8]. Recently, it has also been proposed as a probe for topological superconductivity [9–11], which requires gateable semiconductor Josephson junctions [12].

In contrast to superconductor-insulator-superconductor (SIS) junctions, Josephson junctions with a semiconductor channel feature conductive modes of finite transmission probabilities [13,14], leading to deviations from a sinusoidal current-phase relationship [15] and the universal ratio of the critical current and the normal-state conductance [2]. Furthermore, soft-gap effects [16] have been shown to result in excess quasiparticle current for subgap bias voltages, limiting prospective applications such as topological circuits [17] and gate-controlled transmon qubits [18].

Here we investigate the high-frequency radiation signatures of a voltage-biased semiconductor Josephson junction [12] by directly measuring the frequency-resolved spectral density. As a frequency-sensitive detector, we utilize a SIS junction, where the photon-assisted tunneling current [5] is determined by the spectral density of the coupled microwave radiation [19]. In addition to the detection of the monochromatic Josephson radiation, we demonstrate the presence of a broadband contribution, attributed to the shot noise of the nanowire junction [20], similarly to earlier experiments on carbon nanotube quantum dots [21,22].

Our setup follows the geometry of earlier experiments utilizing SIS junctions [5]. In contrast, our microwave radiation source is an InSb nanowire (NW) [23] Josephson junction [Fig. 1(d)] with a channel length of 100 nm. The junction leads [in brown in Fig. 1(d)] are created by removing the surface oxides by Ar ion milling and then *in situ* sputtering of NbTiN superconducting alloy. Owing to the highly transparent contacts, this procedure enables induced superconductivity in the semiconductor channel [17,18]. A predefined gate structure [purple regions in Fig. 1(d)] provides electrostatic control of the semiconductor channel and is covered by sputtering a 20-nm-thick SiN_x dielectric layer.

The $I(V)$ characteristics of the two junctions are measured in a standard four-point probe geometry via highly resistive Pt feedlines effectively decoupling the on-chip elements (Fig. 1) thermally anchored at 20 mK from the measurement setup. In order to gain access to a wider V_{NW} range, we use $R_1 = 1\ \text{k}\Omega$ in the nanowire biasing lines and $R_2 = 6\ \text{k}\Omega$ in the voltage measurement leads [see Fig. 1(b)].

The detector SIS split junction is shown in Fig. 1(f) and is fabricated using standard shadow evaporation techniques [24]. The typical normal-state resistance was measured to be 20 kΩ for a nominal junction area of $100 \times 100\ \text{nm}^2$. The bottom and top Al layer thicknesses are 9 and 11 nm, respectively. The split junction geometry enables the flux control of the total Josephson coupling of the detector. To measure the quasiparticle tunneling response, we set $\Phi = \Phi_0/2$, with $\Phi_0 = h/2e$ the flux quantum, to minimize the Josephson coupling. We note that the minimal detector critical current is negligible compared to that of the nanowire junction. Finally, we utilize two parallel plate capacitors of $C_c \approx 400$ fF with sputtered SiN_x dielectric which couple the nanowire junction to the detector in the frequencies of interest [Fig. 1(e)], yet enable independent voltage biasing and current measurements in the dc domain.

The mesoscopic noise source under consideration is characterized by its current noise density, $S_I(f)$ [20], which results in the voltage noise density $S_V(f) = S_I(f)|Z(f)|^2$, where $Z(f)$ is the complex frequency-dependent impedance of the coupling circuit. In Fig. 1(b), we depict a parallel RC network resulting in $Z(f) = R(1 - jf/f_0)/(1 + f^2/f_0^2)$ with $2\pi f_0 = (RC)^{-1}$ in the limit of negligible detector admittance, $r_{\text{det}}^{-1} = dI_{\text{det}}/dV_{\text{det}} \ll R^{-1}$.

*Corresponding author: a.geresdi@tudelft.nl

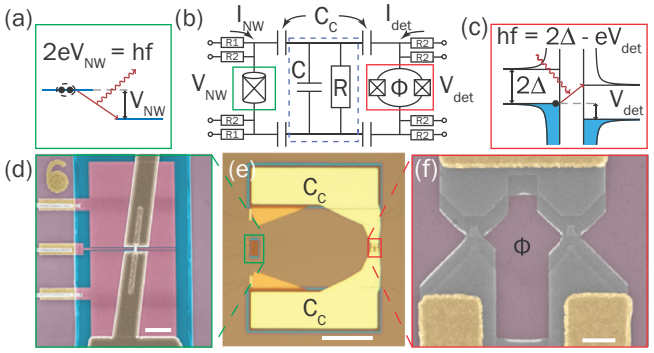

FIG. 1. (a) Photon emission due to the inelastic Cooper-pair tunneling between condensate levels shifted by the bias voltage, V_{NW}. (b) The microwave equivalent circuit of the measurement setup, where R and C in the blue dashed box represent the microwave losses and stray capacitance, yielding a $2\pi f_0 = (RC)^{-1}$ upper cutoff frequency. The $C_c \gg C$ coupling capacitors have a negligible effect above a frequency of $2\pi f_c = (RC_c)^{-1}$ with $f_c \ll f_0$, but allow for the application of independent dc bias voltages V_{NW} and V_{det}. The $I_{\mathrm{NW}}(V_{\mathrm{NW}})$ and $I_{\mathrm{det}}(V_{\mathrm{det}})$ characteristics are measured through the Pt feedline resistors, depicted by R_1 and R_2, respectively. (c) Photon-assisted quasiparticle tunneling for a detector voltage bias V_{det} and an incoming photon energy of hf. (d) False colored scanning electron micrograph of the nanowire Josephson junction contacted with NbTiN after being placed on three electrostatic gates. (e) Bright field optical image of the coupling circuitry before the NbTiN deposition step with the nanowire junction (green box) and the detector junction (red box). (f) False colored micrograph of the detector split junction with an applied magnetic flux Φ. The scale bars depict 1 μm (d), 20 μm (e), and 0.5 μm (f), respectively.

We deduce the voltage noise density $S_V(f)$ starting from the equation for the photon-assisted current in the SIS detector [5,25]:

$$I_{\mathrm{PAT}}(V_{\mathrm{det}}) = \int_0^\infty S_V(f)\left(\frac{e}{hf}\right)^2 I_{QP,0}\left(V_{\mathrm{det}} + \frac{hf}{e}\right)df, \quad (2)$$

which describes the dc current contribution at an applied voltage $V_{\mathrm{det}} < 2\Delta$. Crucially, this equation holds if the quasiparticle current in the absence of radiation has a well-defined onset, $I_{QP,0}(V_{\mathrm{det}} < 2\Delta) = 0$ [5] and in the limit of weak coupling, where multiphoton processes do not contribute to the quasiparticle current [19]. In addition, a detector with a sharp quasiparticle current onset can reach the quantum limit [25] where each absorbed photon results in the tunneling of one quasiparticle.

In the presence of a monochromatic radiation, where $S_V(f) \sim \delta(f - \mathcal{F})$, Eq. (2) describes the shift of the initial $I_{QP,0}(V_{\mathrm{det}})$ quasiparticle current by $\delta V_{\mathrm{det}} = h\mathcal{F}/e$. This is the case of the Josephson radiation [5] with $S_I(f) = \frac{I_c^2}{4}\delta(f - \mathcal{F})$, where $h\mathcal{F} = 2eV_{\mathrm{NW}}$ with V_{NW} the applied voltage bias on the emitter junction with a critical current I_c. On the other hand, the *nonsymmetrized* quasiparticle shot noise is characterized by $S_I = eIF$ in the zero-frequency and zero-temperature limit with I being the applied current. The Fano factor, F, is characteristic to the mesoscopic details of the junction [20].

Note that Eq. (2) can be handled as a convolution of $S_V(f)/(hf)^2$ and $I_{QP,0}(V_{\mathrm{det}})$. However, the inverse problem

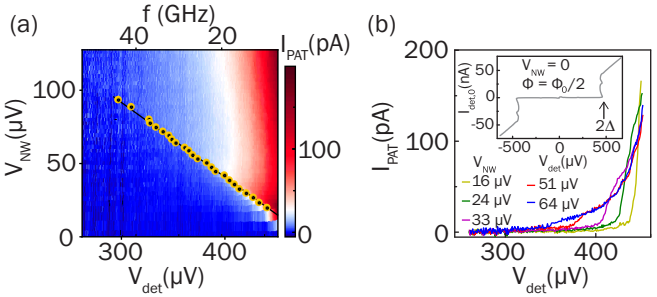

FIG. 2. (a) Measured photon-assisted quasiparticle current I_{PAT} as a function of the detector bias voltage V_{det} and nanowire bias voltage V_{NW}. The orange dots denote the extracted frequency on the upper axis for a given V_{NW}. The solid black line is the best linear fit with $f/V_{\mathrm{NW}} = 475$ MHz/μV. (b) Horizontal line traces at different V_{NW} values. The inset shows the full $I_{\mathrm{det},0}(V_{\mathrm{det}})$ characteristics of the detector when the Josephson radiation is absent. Note the difference in the current scale. The applied flux $\Phi = \Phi_0/2$ through the split junction results in a suppressed detector supercurrent branch which minimizes its Josephson radiation. The arrow depicts $2\Delta/e = 480$ μV, the onset of the quasiparticle current.

leading to $S_V(f)$ is unstable due to the noise in the experimental data. To this end, we use Tikhonov regularization [26] to extract the noise density measured by the detector (see [27] for details). It is to be noted that the measured $I_{\mathrm{det},0}$ [see inset of Fig. 2(b)] exhibits backbending due to the self-heating effects in the leads of the superconducting tunnel junction, therefore we used a monotonous $I_{QP,0}(V_{\mathrm{det}})$ centered around the same quasiparticle onset. However, the uncertainty of $I_{QP,0}(V_{\mathrm{det}})$ prevents the determination of the exact line shape of $S_V(f)$ which could indicate the linewidth of the Josephson radiation [28].

We demonstrate the detection of the Josephson radiation in Fig. 2. In panel (a), we plot the PAT current contribution as a function of the dc bias voltages V_{det} and V_{NW}. In Fig. 2(b), we show line traces $I_{\mathrm{PAT}}(V_{\mathrm{det}})$ exhibiting well-defined onset values corresponding to a monochromatic Josephson radiation tuned by V_{NW}. Thus, we can extract the radiation frequency based on Eq. (2) [orange dots in Fig. 2(a)]. By evaluating the relation between V_{NW} and the radiation frequency [black line in Fig. 2(a)], we find a ratio of $475 \pm 4.2\frac{\mathrm{MHz}}{\mu\mathrm{V}}$ which is in reasonable agreement with $\frac{2e}{h} \sim 484\frac{\mathrm{MHz}}{\mu\mathrm{V}}$ expected for the case of Cooper-pair tunneling [29]. The intersect for $f = 0$ is set by the quasiparticle current onset to be $2\Delta/e = 480$ μV [see inset of Fig. 2(b)].

The impedance $Z(f)$ of the environment results in a finite power dissipation $I_c^2\mathrm{Re}[Z(f)]/2$ which gives rise to a dc current due to inelastic Cooper-pair tunneling (ICPT) processes in the NW Josephson junction [see Fig. 1(a)] [4]. This effect has been first addressed to calculate the shape of the supercurrent branch in overdamped SIS junctions and purely resistive environments [30]. Later, the theory was adapted for high channel transmissions [31]. It has also been shown that for an arbitrary $Z(f) \ll h/4e^2 \approx 6.5$ kΩ, the ICPT contribution can be evaluated as [4]

$$I_{\mathrm{ICPT}} = \frac{I_c^2\mathrm{Re}[Z(f)]}{2V_{\mathrm{NW}}}, \quad (3)$$

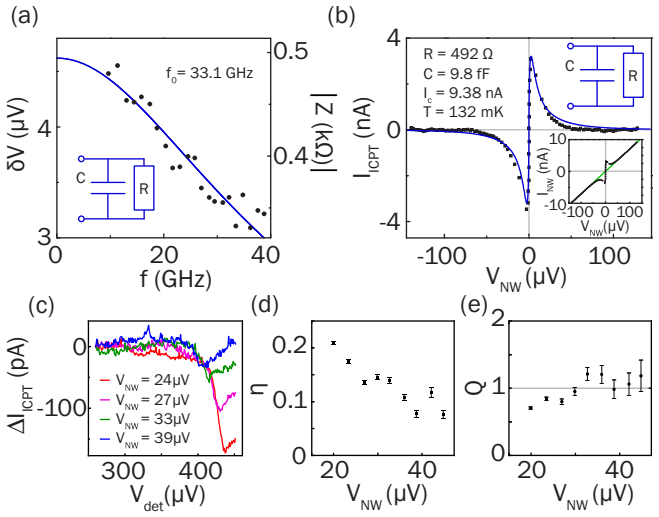

FIG. 3. (a) The measured $\delta V(f) = I_c|Z(f)|$ voltage fluctuation on the detector junction. The solid line depicts the fitted cutoff with $f_0 = (2\pi RC)^{-1} = 33.1$ GHz. Right vertical axis shows the impedance $|Z(f)|$ (see text). (b) Experimental $I_{\rm ICPT}(V_{\rm NW})$ trace of the nanowire junction exhibiting a current peak due to the supercurrent branch. The linear contribution with a resistance $R_{\rm NW} = 14.03$ kΩ [green solid line; see inset for raw $I_{\rm NW}(V_{\rm NW})$ trace] is subtracted. The blue solid line depicts the fitted curve with $I_c = 9.38$ nA critical current and a noise temperature $T = 132$ mK. (c) Variation of the nanowire junction current $\Delta I_{\rm ICPT}$ as a function of the detector voltage $V_{\rm det}$. The extracted circuit efficiency η (d) and the detector quantum efficiency Q (e) as a function of $V_{\rm NW}$ (see text).

with a critical current I_c and an applied voltage $V_{\rm NW}$. Here, the junction effectively probes the real component of the impedance $Z(f)$ at a frequency $f = 2eV_{\rm NW}/h$.

In the following, we use a circuit model where the two independently measured current values $I_{\rm PAT}(V_{\rm det})$ and $I_{\rm ICPT}(V_{\rm NW})$ depend on the same microwave enviroment, characterized by $Z(f)$. This model applies provided that the linear resistance of the nanowire and the impedance of the detector, $r_{\rm det}$, are much higher than the effective shunt resistance of the circuit, depicted by R in Fig. 1(b). In addition, the lumped element description of Fig. 1(b) is valid if the circuit is much smaller than the characteristic wavelength $c/f \sim 1$ mm. Our structure, 50 μm in size [see Fig. 1(e)], fulfills this condition. Note that this is in contrast to a prior work [8] where the sample and detector were embedded in a transmission line resonator and thus the effective impedance values were measured to be different.

It is important to notice that the PAT current decreases with increasing frequency [Fig. 2(b)]. By correcting for the $\sim f^{-2}$ dependence in Eq. (2), we find that the fluctuation amplitude $\delta V = I_c|Z(f)| \sim \sqrt{S_V}$ exhibits a characteristic cutoff frequency [Fig. 3(a)], even though the current oscillation amplitude of the Josephson junction is constant [see Eq. (1)]. Thus, we can attribute this cutoff to the coupling circuit impedance, $Z(f)$. We find a good agreement between the experimental data and the impedance of a single-pole RC network [solid blue line in Fig. 3(a)] yielding to a cutoff frequency $f_0 = (2\pi RC)^{-1} = 33.1$ GHz.

Next, we turn to the measured $I(V)$ trace of the nanowire Josephson junction. The inset of Fig. 3(b) shows the raw curve, which exhibits a supercurrent peak around zero $V_{\rm NW}$ and a linear branch. The latter fits to a linear slope of $R_{\rm NW} = 14.03$ kΩ (solid green line). We then extract the $I_{\rm ICPT}(V_{\rm NW})$ component by subtracting this slope from the raw measured data [black dots in Fig. 3(b)], which is an additive component to the supercurrent peak unless the device has channels of transmission very close to unity [31]. In order to find the critical current and the noise temperature of the junction, we use the finite temperature solution of Ivanchenko and Zil'bermann [30] with substituting $|Z(f)|$ as the impedance of the environment [27]. With this addition, we find an excellent agreement with the experimental data [blue solid line in Fig. 3(b)], with $I_c = 9.38$ nA critical current. Notably, with the now determined value of I_c, we can extract $R = 492$ Ω and $C = 9.8$ fF fully characterizing the microwave environment of the junctions. In addition, we find $I_c R_{\rm NW} = 132$ μV, which indicates the induced superconducting gap in the nanowire channel. This value is close to the induced gap values measured earlier in similar devices [17,32]. We also extract an effective noise temperature $T = 132$ mK, which is higher than the substrate temperature of 20 mK, similarly to earlier experiments [31].

Thus far, we evaluated $I_{\rm ICPT}(V_{\rm NW})$ at $V_{\rm det} \approx 50\ \mu{\rm V} \ll 2\Delta/e = 480\ \mu$V, where $I_{\rm PAT} \approx 0$, thus the detector load is negligible. However, depending on $V_{\rm NW}$, we find a negative $\Delta I_{\rm ICPT}(V_{\rm det})$, i.e., a reduction of the emitter current, when the detector threshold is on resonance with the emitted frequency [Fig. 3(c)]. We can understand this effect by the reduction of $Z(f)$ in Eq. (3) in the presence of a finite $r_{\rm det}$ in parallel with R. In first order, we find $\Delta I_{\rm ICPT}/I_{\rm ICPT} = -{\rm Re}[Z(f)]/r_{\rm det} \approx -R/r_{\rm det}$. By using the measured dc current values, we evaluate the efficiency of the coupling circuit to be the ratio of the absorbed and emitted power $\eta = P_{\rm det}/P_{\rm emi} = 2I_{\rm PAT}/I_{\rm ICPT}$ [Fig. 3(d)]. We find typical values spanning 0.1–0.2, an order of magnitude improvement over earlier reported values [5,33], however, $\eta < 1$ owing to the resistive losses of the device. Furthermore, the decrease of η with increasing f is consistent with the low-pass nature of the coupling circuit. We also calculate the detector quantum efficiency $Q = P_{\rm det}/\Delta P_{\rm emi} = 2I_{\rm PAT}/\Delta I_{\rm ICPT}$ [Fig. 3(e)] and find values scattering around

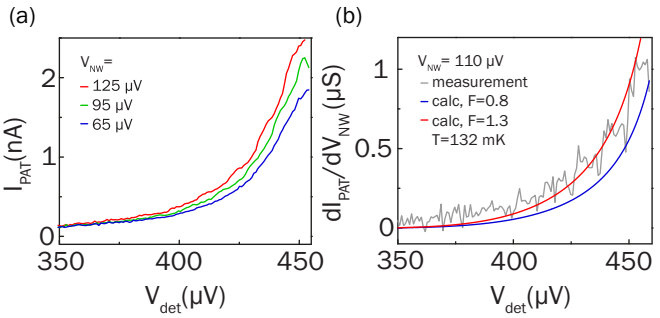

FIG. 4. (a) Measured detector $I_{\rm PAT}(V_{\rm det})$ line traces at $V_{\rm NW} = 65$, 95, and 125 μV bias voltage from the bottom to top, respectively. (b) The measured $dI_{\rm PAT}/dV_{\rm NW}$ (light-gray line) and the fitted curves at the top ($F = 1.3$, red line) and the bottom ($F = 0.8$, blue line) of the confidence interval, respectively.

unity. This value directly measures the ratio of electron and photon rate passing the detector junction, thus confirming that it is in the quantum limit [25].

Finally, we note that the measured reduction $\Delta I_{\mathrm{ICPT}}/I_{\mathrm{ICPT}} \ll 1$ directly confirms our initial assumption of negligible detector load on the circuit. This proves that the analysis based on a circuit model with the same $Z(f)$ for the nanowire junction and the SIS detector is consistent.

We now turn to the shot-noise contribution to I_{PAT}. We observe a monotonous increase in I_{PAT} with increasing V_{NW} at any V_{det} consistently with the broadband S_I [Fig. 4(a)]. Note that, in contrast with the data shown in Fig. 2(b), here the contribution of the Josephson radiation is negligible. To quantify the shot-noise contribution, we consider the derivative of the nonsymmetrized expression with respect to V_{NW} [34]:

$$\frac{dS_I(f)}{dV_{\mathrm{NW}}} = \frac{F}{R_{\mathrm{qp}}}\frac{d}{dV_{\mathrm{NW}}}\left(\frac{hf+eV_{\mathrm{NW}}}{1-e^{-\beta(hf+eV_{\mathrm{NW}})}}+\frac{hf-eV_{\mathrm{NW}}}{1-e^{-\beta(hf-eV_{\mathrm{NW}})}}\right), \tag{4}$$

where $\beta = 1/k_{\mathrm{B}}T$ is the inverse temperature [35]. We can then calculate $dI_{\mathrm{PAT}}/dV_{\mathrm{NW}}$ by subsituting $dS_I(f)/dV_{\mathrm{NW}}$ in place of $S_I(f)$ in Eq. (2). Using the effective temperature $T = 132$ mK extracted earlier we find a confidence interval of $F = 0.8 \ldots 1.3$ [Fig. 4(b)]. Considering that the channel length of 100 nm is similar to the mean free path found earlier in the same nanowires [36], this result is consistent with ballistic transport which is dominated by single electron channels of low transmission where $F = 1$ [20,37]. In contrast, $F = 1/3$ characteristic of diffusive normal transport [38] does not fit our data.

Furthermore, the measured $I_{\mathrm{NW}}(V_{\mathrm{NW}})$ and $I_{\mathrm{PAT}}(V_{\mathrm{NW}})$ do not agree with a transport dominated by multiple Andreev reflections, where a subgap structure is anticipated both in the current [39] and in the shot noise [40] depending on the channel transmissions. Our experiment thus provides insight into the nature of the charge transport at finite voltage bias in the nanowire Josephson junction and concludes that the finite subgap current can be attributed to single electron states inside the induced superconducting gap.

In conclusion, we built and characterized an on-chip microwave coupling circuit to measure the microwave radiation spectrum of an InSb nanowire junction with NbTiN bulk superconducting leads. Our results clearly demonstrate the possibility of measuring the frequency of the Josephson radiation in a wide frequency range, opening new avenues in investigating the 4π-periodic Josephson effect [41] in the context of topological superconductivity [42]. Based on the Fano factor, the shot-noise contribution to the measured signal demonstrates the presence of subgap quasiparticle states and excludes multiple Andreev reflection as the source of subgap current of the nanowire Josephson junction.

ACKNOWLEDGMENTS

The authors acknowledge D. Bouman, A. Bruno, O. Benningshof, M. C. Cassidy, M. Quintero-Pèrez, and R. Schouten for technical assistance and R. Deblock for fruitful discussions. This work has been supported by the Dutch Organization for Fundamental Research on Matter (FOM), the Netherlands Organization for Scientific Research (NWO) by a Veni grant, Microsoft Corporation Station Q, and a Synergy Grant of the European Research Council.

[1] B. D. Josephson, Phys. Lett. **1**, 251 (1962).
[2] V. Ambegaokar and A. Baratoff, Phys. Rev. Lett. **10**, 486 (1963).
[3] I. Giaever, Phys. Rev. Lett. **14**, 904 (1965).
[4] T. Holst, D. Esteve, C. Urbina, and M. H. Devoret, Phys. Rev. Lett. **73**, 3455 (1994).
[5] R. Deblock, E. Onac, L. Gurevich, and L. P. Kouwenhoven, Science **301**, 203 (2003).
[6] P.-M. Billangeon, F. Pierre, H. Bouchiat, and R. Deblock, Phys. Rev. Lett. **98**, 216802 (2007).
[7] M. Hofheinz, F. Portier, Q. Baudouin, P. Joyez, D. Vion, P. Bertet, P. Roche, and D. Esteve, Phys. Rev. Lett. **106**, 217005 (2011).
[8] J. Basset, H. Bouchiat, and R. Deblock, Phys. Rev. B **85**, 085435 (2012).
[9] D. I. Pikulin and Y. V. Nazarov, Phys. Rev. B **86**, 140504 (2012).
[10] P. San-Jose, E. Prada, and R. Aguado, Phys. Rev. Lett. **108**, 257001 (2012).
[11] M. Houzet, J. S. Meyer, D. M. Badiane, and L. I. Glazman, Phys. Rev. Lett. **111**, 046401 (2013).
[12] Y.-J. Doh, J. A. van Dam, A. L. Roest, E. P. A. M. Bakkers, L. P. Kouwenhoven, and S. De Franceschi, Science **309**, 272 (2005).
[13] J. Xiang, A. Vidan, M. Tinkham, R. M. Westervelt, and C. M. Lieber, Nat. Nanotechnol. **1**, 208 (2006).
[14] D. J. van Woerkom, A. Proutski, B. van Heck, D. Bouman, J. I. Väyrynen, L. I. Glazman, P. Krogstrup, J. Nygård, L. P. Kouwenhoven, and A. Geresdi, Nat. Phys. **13**, 876 (2017).
[15] M. L. D. Rocca, M. Chauvin, B. Huard, H. Pothier, D. Esteve, and C. Urbina, Phys. Rev. Lett. **99**, 127005 (2007).
[16] S. Takei, B. M. Fregoso, H.-Y. Hui, A. M. Lobos, and S. D. Sarma, Phys. Rev. Lett. **110**, 186803 (2013).
[17] V. Mourik, K. Zuo, S. M. Frolov, S. R. Plissard, E. P. A. M. Bakkers, and L. P. Kouwenhoven, Science **336**, 1003 (2012).
[18] G. de Lange, B. van Heck, A. Bruno, D. J. van Woerkom, A. Geresdi, S. R. Plissard, E. P. A. M. Bakkers, A. R. Akhmerov, and L. DiCarlo, Phys. Rev. Lett. **115**, 127002 (2015).
[19] P. K. Tien and J. P. Gordon, Phys. Rev. **129**, 647 (1963).
[20] Y. M. Blanter and M. Büttiker, Phys. Rep. **336**, 1 (2000).
[21] E. Onac, F. Balestro, B. Trauzettel, C. F. J. Lodewijk, and L. P. Kouwenhoven, Phys. Rev. Lett. **96**, 026803 (2006).
[22] J. Basset, A. Y. Kasumov, C. P. Moca, G. Zaránd, P. Simon, H. Bouchiat, and R. Deblock, Phys. Rev. Lett. **108**, 046802 (2012).
[23] S. R. Plissard, D. R. Slapak, M. A. Verheijen, M. Hocevar, G. W. G. Immink, I. van Weperen, S. Nadj-Perge, S. M. Frolov, L. P. Kouwenhoven, and E. P. A. M. Bakkers, Nano Lett. **12**, 1794 (2012).
[24] G. Dolan, Appl. Phys. Lett. **31**, 337 (1977).
[25] J. R. Tucker and M. J. Feldman, Rev. Mod. Phys. **57**, 1055 (1985).

[26] D. D. Trong, C. X. Phuong, T. T. Tuyen, and D. N. Thanh, Commun. Stat. Theory Methods **43**, 4384 (2014).
[27] Raw data and calculations, doi:10.4121/uuid:2cfc62ff-e15e-4e90-90e1-e6254baecb12.
[28] A. J. Dahm, A. Denenstein, D. N. Langenberg, W. H. Parker, D. Rogovin, and D. J. Scalapino, Phys. Rev. Lett. **22**, 1416 (1969).
[29] W. H. Parker, B. N. Taylor, and D. N. Langenberg, Phys. Rev. Lett. **18**, 287 (1967).
[30] Yu. M. Ivanchenko and L. A. Zil'berman, Zh. Eksp. Teor. Fiz. **55**, 2395 (1968) [Sov. Phys. JETP **28**, 1272 (1969)].
[31] M. Chauvin, P. vom Stein, D. Esteve, C. Urbina, J. C. Cuevas, and A. L. Yeyati, Phys. Rev. Lett. **99**, 067008 (2007).
[32] Ö. Gül, H. Zhang, F. K. de Vries, J. van Veen, K. Zuo, V. Mourik, S. Conesa-Boj, M. P. Nowak, D. J. van Woerkom, M. Quintero-Pérez, M. C. Cassidy, A. Geresdi, S. Koelling, D. Car, S. R. Plissard, E. P. A. M. Bakkers, and L. P. Kouwenhoven, Nano Lett. **17**, 2690 (2017).
[33] P.-M. Billangeon, F. Pierre, H. Bouchiat, and R. Deblock, Phys. Rev. Lett. **96**, 136804 (2006).
[34] R. Aguado and L. P. Kouwenhoven, Phys. Rev. Lett. **84**, 1986 (2000).
[35] Note that we omitted the voltage-independent terms in [34].
[36] Ö. Gül, D. J. van Woerkom, I. van Weperen, D. Car, S. R. Plissard, E. P. Bakkers, and L. P. Kouwenhoven, Nanotechnology **26**, 215202 (2015).
[37] M. de Jong and C. W. J. Beenakker, in *Mesoscopic Electron Transport*, edited by L. Sohn and L. Kouwenhoven (Kluwer, The Netherlands, 1997).
[38] C. W. J. Beenakker and M. Büttiker, Phys. Rev. B **46**, 1889 (1992).
[39] E. Scheer, P. Joyez, D. Esteve, C. Urbina, and M. H. Devoret, Phys. Rev. Lett. **78**, 3535 (1997).
[40] R. Cron, M. F. Goffman, D. Esteve, and C. Urbina, Phys. Rev. Lett. **86**, 4104 (2001).
[41] R. M. Lutchyn, J. D. Sau, and S. D. Sarma, Phys. Rev. Lett. **105**, 077001 (2010).
[42] Y. Oreg, G. Refael, and F. von Oppen, Phys. Rev. Lett. **105**, 177002 (2010).